

OPEN

Scalable radiative thermal logic gates based on nanoparticle networks

Christoph Kathmann¹, Marta Reina², Riccardo Messina², Philippe Ben-Abdallah² & Svend-Age Biehs^{1*}

We discuss the design of the thermal analog of logic gates in systems made of a collection of nanoparticles. We demonstrate the possibility to perform NOT, OR, NOR, AND and NAND logical operations at submicrometric scale by controlling the near-field radiative heat exchanges between their components. We also address the important point of the role played by the inherent non-additivity of radiative heat transfer in the combination of logic gates. These results pave the way to the development of compact thermal circuits for information processing and thermal management.

In electronics a logic gate is a circuit which implements a Boolean operation from input digits based on an electric signal with distinct discrete levels. Non-electronic devices have been proposed during the last decades to perform such Boolean treatment without electric power source. Hence, purely optical¹, mechanical² and even biological devices^{3,4} have been developed to process information without electric current. In 2007 the idea of basic thermal logic gates⁵ has been introduced, in order to make logical operations using temperature differences and heat flux carried by acoustic phonons in non-linear solid circuits as an alternative to electric circuits.

Since the beginning of 2000's, the possibility to control the radiative heat exchanges at the nanoscale between two or several objects mechanically^{6–8}, electrically and chemically^{9–13}, or with external magnetic fields^{14–20} has been demonstrated, opening so promising prospects in this domain as well as in the field of thermal management.

As a result, non-linear two-body devices have been first proposed to rectify heat flux both in near-field and in far-field regimes^{21–33}, allowing thus the fabrication of true radiative thermal diodes. More recently, three-terminal systems have unveiled the possibility to store and to amplify the thermal energy carried by thermal photons opening the door to the realization of radiative memories and transistors^{23,24,34–39}. This paves the way to thermal circuits to control heat flow at nanoscale in a similar way as in modern electronics⁴⁰.

These recent results, promising in the direction of information treatment with thermal photons and thermal management in general, suffer of two main limitation. The first is that the planar geometry considered so far does not leave much room for both down-sizing of the device and geometrical arrangement in order to combine different ports and realize more elaborate thermal circuits. The second limitation is that only NOT, OR and AND gates have been demonstrated so far. In order to overcome the first drawback, we address here the problem of the design of thermal logic gates based on nanoparticles. These systems, which are nowadays experimentally feasible, remove the constraint of a 1D arrangement, paving the way to an easier combination of logic ports. Moreover, the dipolar approximation allows for a relatively easy theoretical treatment of heat exchange in these systems. For this configuration, we extend our previous work on basic logic ports and we design NOT, OR, NOR, AND and NAND logic ports. We also discuss the important problem of how the inherent non-additivity of radiative heat transfer affects the combination of several ports together and address the scalability of the designed logic ports.

Methods

Theoretical framework. To explore theoretically the possibility to realize different logic gates and their combination we restrict ourselves to many-body systems consisting of N spherical nanoparticles in vacuum, for convenience. These nanoparticles will serve as the input/output terminals of the logic gates and are treated within the dipole model which can be safely used when the particle radii are much smaller than the interparticle distances⁴¹. In this case, the power received by a particle i at a temperature T_i through heat radiation from particle j with temperature T_j in the presence of all other $N - 2$ particles can be expressed by^{42–44}

¹Institut für Physik, Carl von Ossietzky Universität, D-26111, Oldenburg, Germany. ²Laboratoire Charles Fabry, UMR 8501, Institut d'Optique, CNRS, Université Paris-Sud 11, 2, Avenue Augustin Fresnel, 91127, Palaiseau, Cedex, France. *email: s.age.biehs@uni-oldenburg.de

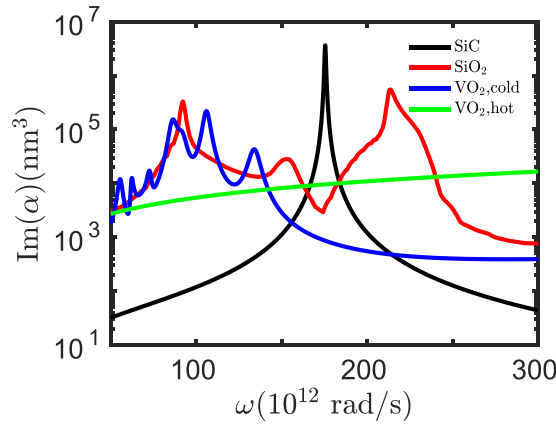


Figure 1. Particle absorptivity. Plot of $\text{Im}(\alpha)$ for spherical SiC and VO_2 nanoparticles with radius $a = 25$ nm.

$$P_{j \rightarrow i} = \int_0^\infty \frac{d\omega}{2\pi} \frac{\text{Im}(\alpha_i)\text{Im}(\alpha_j)}{|\alpha_j|^2} \Theta_{ji} \text{Tr} \left(\mathbb{T}_{ij}^{-1} \mathbb{T}_{ji}^{-1} \right), \quad (1)$$

with

$$\Theta_{ji} = \frac{\hbar\omega}{e^{\hbar\omega/k_B T_j} - 1} - \frac{\hbar\omega}{e^{\hbar\omega/k_B T_i} - 1}, \quad (2)$$

introducing the reduced Planck constant \hbar and the Boltzmann constant k_B . The transferred power depends on the product of the imaginary parts of the two particles. For a given spherical particle i we take the Clausius-Mossotti expression of the polarizability

$$\alpha_i = 4\pi a_i^3 \frac{\epsilon_i - 1}{\epsilon_i + 2} \quad (3)$$

where a_i is the radius and ϵ_i is the permittivity of particle i . Furthermore the exchanged power depends on the matrix \mathbb{T} which is a $3N \times 3N$ block matrix with components defined by⁴²

$$\mathbb{T}_{ij} = \delta_{ij} - (\delta_{ij} - 1) \frac{\omega^2}{c^2} \alpha_i \mathbb{G}^{(0)}(\mathbf{r}_i, \mathbf{r}_j). \quad (4)$$

Here, $\mathbb{G}^{(0)}(\mathbf{r}_i, \mathbf{r}_j)$ is the well-known Green's dyadic in vacuum⁴⁵ evaluated at the positions $\mathbf{r}_{i/j}$ of particle i/j and c is the vacuum light velocity. Effects like the coupling to surface modes of a nearby substrate as studied in refs.^{46–49} are therefore neglected at this stage. Furthermore, we neglect the heat flux between the particles and the surrounding environment, which itself provides a heat flux channel, since this gives a negligible contribution when the particles are interacting in the near field⁴². In agreement with this simplification we also neglect the radiation correction⁵⁰. More important in the following is that through the block matrix \mathbb{T} we take into account all many-body interactions. Note, that the polarizability α is proportional to the particle radius a^3 and the Green's function scales in the near-field regime like $1/d^3$ where $d = |\mathbf{r}_i - \mathbf{r}_j|$ is the distance between two particles. Therefore the second term in the matrix \mathbb{T} scales like $(a/d)^3$ in the near-field regime. Hence, when scaling the radii of all particles and the distances by the same factor, the results remain unchanged. Therefore the whole systems considered in the following can be down- and upscaled without changing the functionalities by multiplying the distances and radii with one scaling factor. The limit for the downscaling is, of course, the validity of the macroscopic approach which can be applied to length scales much larger than the atomic dimensions or the lattice constant of the material where the dielectric constant cannot be defined anymore. Practically speaking this occurs for particles of sub-nanometer radius where quantum effects must be taken into account. The limit for the upscaling is the validity of the dipole approximation and near-field regime. Both are typically valid for radii and distances smaller than 1/10 of the thermal wavelength. For logic gates operating around the ambient temperature this corresponds to sizes larger than a few micrometers. However the higher-order modes (i.e. multipolar contributions) can easily be taken into account to deal with bigger particles. Also the well known proximity approximation could be used to deal with big particles.

Finally, the full power received or emitted by the particle i is given by

$$P_i(T_1, \dots, T_N) = \sum_{j \neq i} P_{j \rightarrow i}. \quad (5)$$

Note that the dipole model offers the possibility to model also more complex geometries for the input and output terminals in a discrete-dipole approximation^{42–44,51–53} which is a huge advantage regarding the constraints imposed by layered media as considered for the construction of transistors and logic gates previously^{34,35,40}.

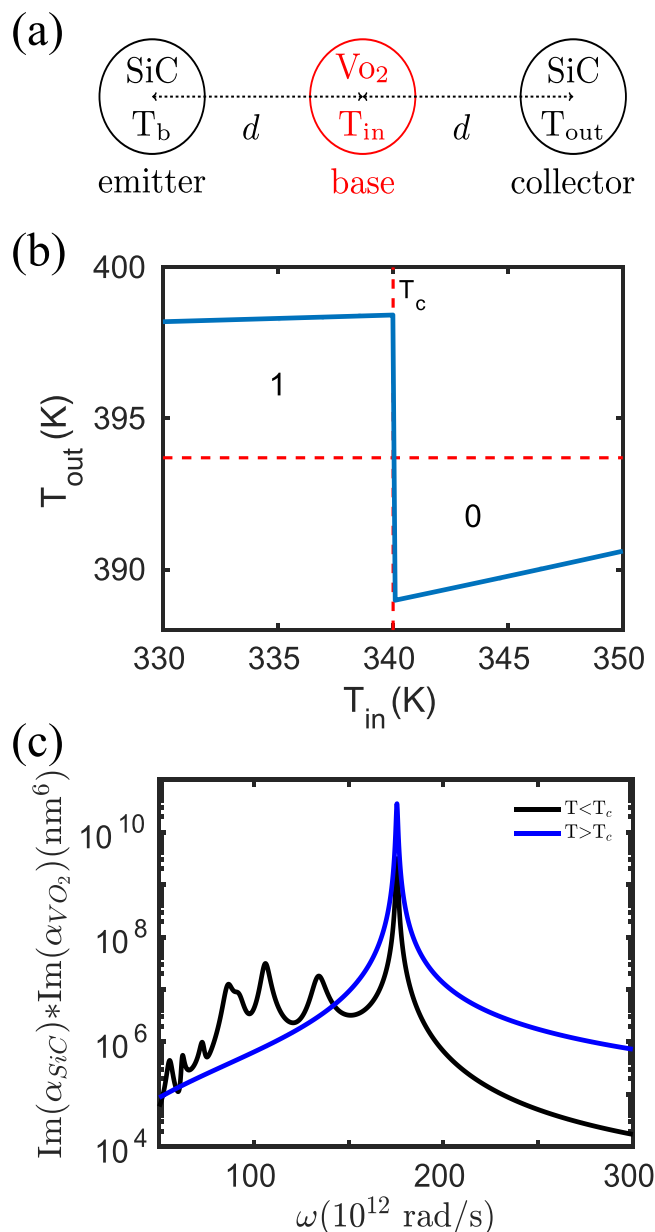


Figure 2. NOT gate. (a) Sketch of the NOT gate configuration. The radius of the nanoparticles is $a = 25$ nm and the interparticle distance is $d = 100$ nm. (b) Output of the NOT gate in (a) when $T_b = 400$ K. The “0” (“1”) of the input is defined by $T_{in} < T_c$ ($T_{in} > T_c$). The “0” (“1”) of the output is defined by $T_{out} < 394$ K ($T_{out} > 394$ K). (c) $\text{Im}(\alpha_{SiC}) * \text{Im}(\alpha_{VO_2})$ for VO₂ in the dielectric (metallic) phase for which $T < T_c$ ($T > T_c$).

Furthermore, the discrete dipole approximation also offers the possibility to design complex and nearly arbitrary circuits for thermal radiation.

Optical properties. In our simulations we will use the optical properties of VO₂, SiO₂ and SiC from literature^{54,55}. These optical properties determine the absorptivity of the particles which is proportional to $\text{Im}(\alpha_i)$ and the coupling strengths which are proportional to $\text{Im}(\alpha_i)\text{Im}(\alpha_j)$. In Fig. 1 we show $\text{Im}(\alpha_i)$ of SiC, SiO₂ and VO₂ nanoparticles. The absorptivity of the SiC particle has a sharp resonance at the position of the localized surface phonon polariton at $\omega = 1.756 \times 10^{14}$ rad/s. Similarly, SiO₂ shows peaks at the phonon polariton resonances around $\omega = 1 \times 10^{14}$ rad/s, $\omega = 1.5 \times 10^{14}$ rad/s, $\omega = 2.1 \times 10^{14}$ rad/s. Now, it is important to note that VO₂ has a sharp phase transition at a critical temperature $T_c = 340$ K from a dielectric ($T < T_c$) to a metallic state ($T > T_c$). In its dielectric state it also supports localized surface mode resonances clearly seen in the spectrum of $\text{Im}(\alpha)$. In the metallic state the absorptivity shows no resonance feature, i.e. there are no localized surface mode resonances in the shown frequency region. It is interesting that for frequencies larger than 1.5×10^{14} rad/s the absorptivity of VO₂ in its metallic state is larger than that of VO₂ in its dielectric state. Furthermore, in the frequency region

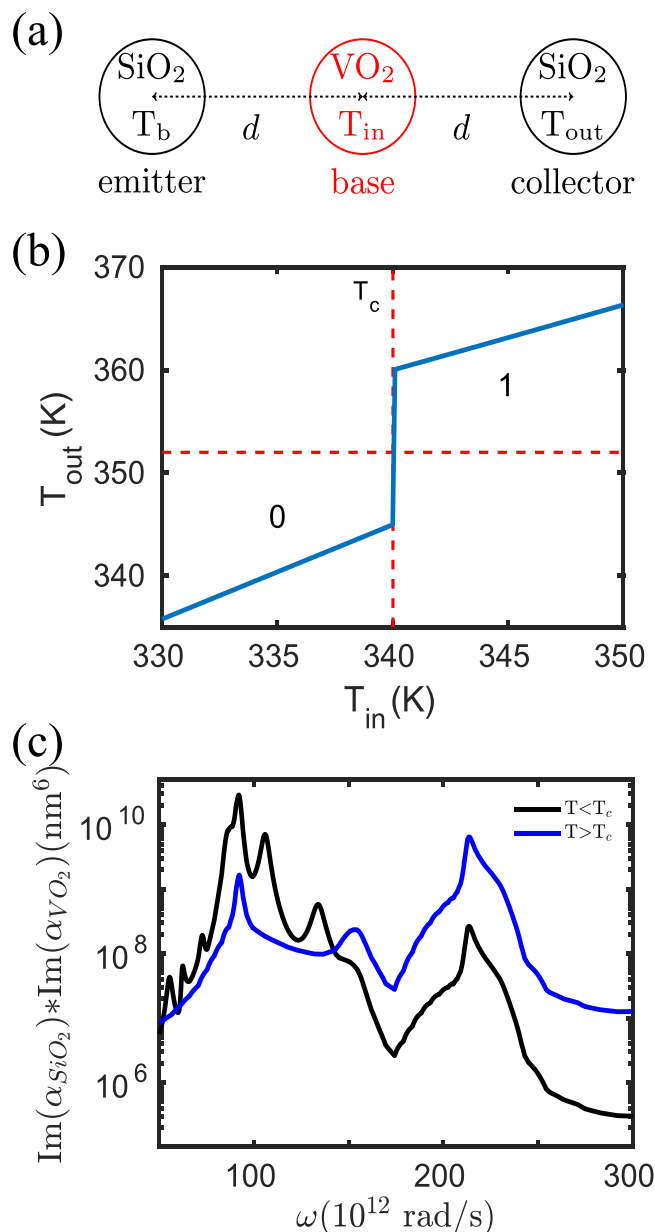


Figure 3. UNIT gate. (a) Sketch of the UNIT gate configuration. The radii of the nanoparticles is $a = 25$ nm and the interparticle distance is $d = 100$ nm. (b) Output of the UNIT gate in (a) when $T_b = 400$ K. The “0” (“1”) of the input is defined by $T_{in} < T_c$ ($T_{in} > T_c$). The “0” (“1”) of the output is defined by $T_{out} < 352$ K ($T_{out} > 352$ K). (c) $\text{Im}(\alpha_{\text{SiO}_2}) \cdot \text{Im}(\alpha_{\text{VO}_2})$ for VO₂ in the dielectric (metallic) phase for which $T < T_c$ ($T > T_c$).

below $\omega = 1.5 \times 10^{14}$ rad/s the phonon-polariton resonances of VO₂ in its dielectric state nicely overlap with the ones of SiO₂.

Results and Discussion

NOT and UNIT gate. We will now use Eq. 1 to simulate the functionalities of logic gates with input/output terminals represented by a nanoparticle. We start with a realization of a NOT gate. To this end, we consider a three-body configuration as depicted in Fig. 2(a) where the collector and the emitter are given by SiC nanoparticles and the base is a VO₂ particle. To operate this NOT gate, we fix the temperature of the emitter at $T_b = 400$ K and take the base particle as the input terminal and the collector particle as the output terminal, i.e. we control the input temperature T_{in} and let the output particle relax into its nonequilibrium steady state. The corresponding output temperature T_{out} is determined by the condition that the full power received or emitted by the collector particle is zero, which can be evaluated numerically, e.g. using Newton’s method, to determine T_{out} such that the power $P_{\text{collector}}(T_b, T_{in}, T_{out}) = 0$ W. The results for T_{out} as a function of T_{in} are shown in Fig. 2(b). It can be seen that at $T_{in} = T_c = 340$ K there is a jump of the output temperature from 398 K to 388 K. Hence, if we define

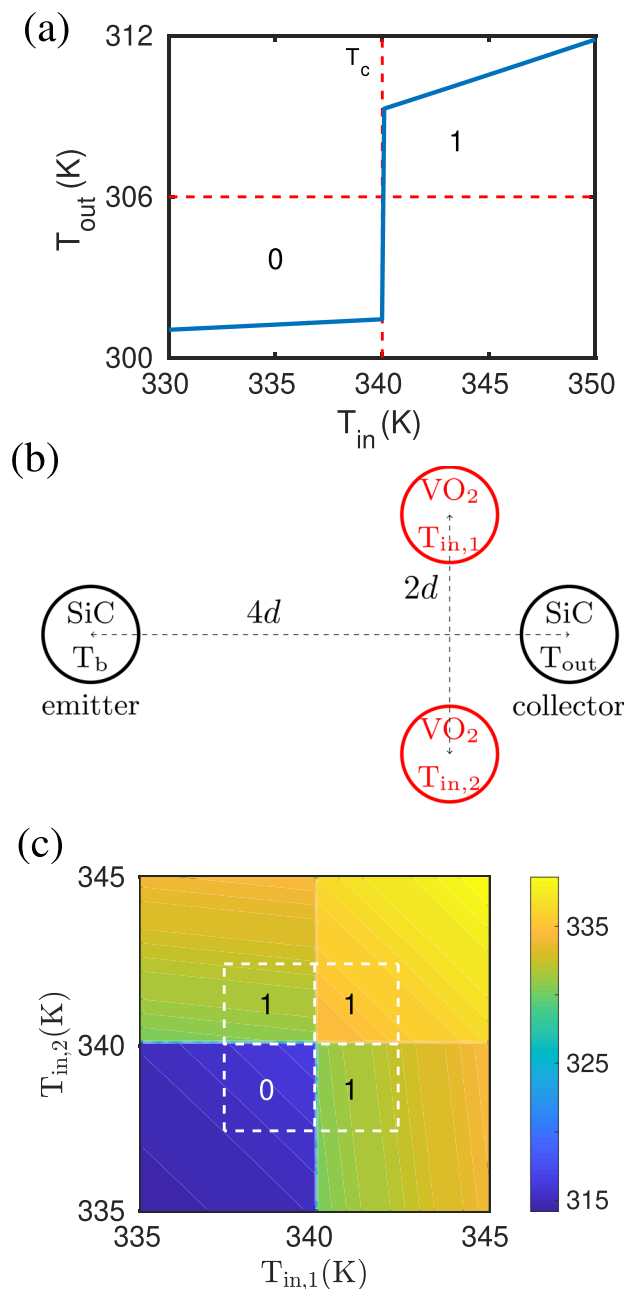


Figure 4. UNIT and OR gate. (a) The output temperature of the configuration in Fig. 2(a) with $T_b = 300$ K. The functionality is that of a UNIT gate for logical operations. (b) Sketch of the OR gate configuration. The radii of the nanoparticles is $a = 25$ nm and the interparticle distance between the two input particles is $2d = 200$ nm and between the emitter and collector particle the distance is $4d = 400$ nm and $T_b = 400$ K. (c) The output temperature of the configuration in (a) with $T_b = 300$ K. The functionality is that of an OR gate.

input temperatures with $T_{in} < 340$ K as “0” and $T_{in} > 340$ K as “1” and correspondingly $T_{out} < 394$ K as “0” and $T_{out} > 394$ K as “1” then we have a realization of a NOT gate.

To understand the physics behind the NOT gate operation, we show in Fig. 2(c) the quantity $\text{Im}(\alpha_{SiC})\text{Im}(\alpha_{VO_2})$ for the case where the VO_2 particle is in its dielectric state ($T < T_c$) and for the metallic state ($T > T_c$). It can be seen that because $\text{Im}(\alpha_{VO_2})$ is for $T > T_c$ larger than for $T < T_c$ at the resonance of the SiC particle in Fig. 1 the coupling between the VO_2 particle and the SiC particle is stronger for $T > T_c$ than for $T < T_c$ as can be seen in Fig. 2(c). Therefore, when the VO_2 particle is in its dielectric phase, the cooling of the output particle by the VO_2 input particle is small. On the other hand, when the VO_2 particle is in its metallic phase the input VO_2 particle has a significant cooling effect on the output particle. This explains why the output particle is hotter for $T_{in} < T_c$ than for $T_{in} > T_c$. The NOT ability is therefore provided by the phase-change of the VO_2 input particle and the corresponding change of the coupling to the output particle.

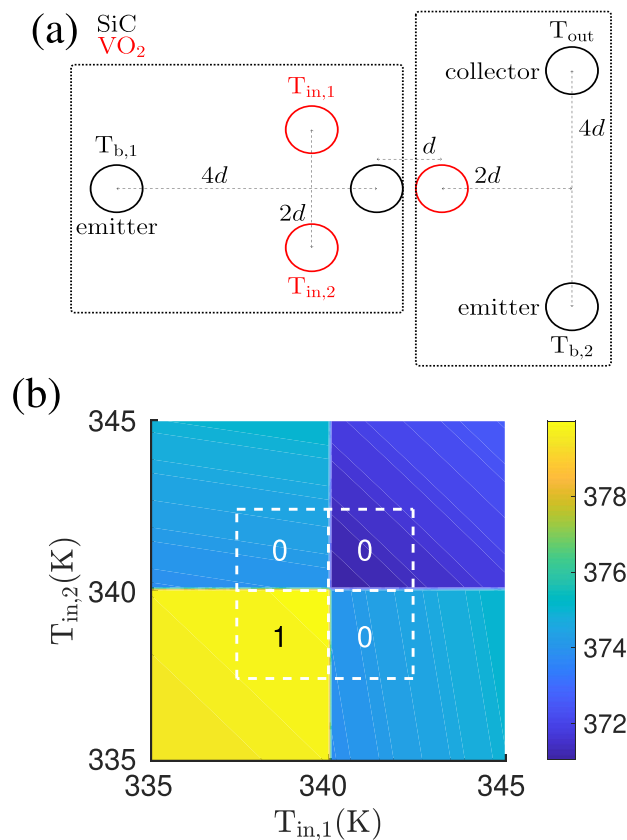


Figure 5. NOT + OR = NOR gate. (a) Sketch of an OR gate coupled to a NOT gate with $T_{b,1} = 300$ K and $T_{b,2} = 400$ K. (b) The output temperature of the NOT + OR gate has the functionality of a NOR gate. Note that this output temperature scheme can also be interpreted as a NAND gate with a slight redefinition of the range of output temperatures for “0” and “1”.

By replacing now the SiC nanoparticles by SiO₂ nanoparticles as shown in Fig. 3(a), we observe in Fig. 3(b) that this configuration functions as a UNIT gate. Again this behaviour can be understood by the coupling strength $\text{Im}(\alpha_{\text{SiO}_2})\text{Im}(\alpha_{\text{VO}_2})$ visualized in Fig. 3(c) where it can be seen that the peaks around $\omega = 1 \times 10^{14}$ rad/s are much larger for $T_{\text{in}} < T_c$ than for $T_{\text{in}} > T_c$. That means, in contrast to the SiC particles, that the SiO₂ particles are well coupled with the VO₂ particles when $T < T_c$ due to the overlap of the localized resonant modes in both particles. On the other hand, for $T > T_c$ the particles are not well coupled so that for $T < T_c$ the VO₂ input particle efficiently cools down the output SiO₂ particle, whereas for $T > T_c$ the cooling of the VO₂ input particle becomes less efficient resulting in the UNIT gate functionality.

It is now interesting to observe that, by operating the NOT gate slightly differently, we can invert its functionalities. More specifically, the output of the NOT gate configuration in Fig. 2(a) is completely changed when the emitter particle temperature T_b is changed from 400 K to 300 K. The output temperature of the NOT gate with $T_b = 300$ K are shown in Fig. 4(a). We clearly see that the functionality is inverted and the NOT gate operates as a UNIT element with respect to the logical operation when defining $T_{\text{out}} < 306$ K as “0” and $T_{\text{out}} > 306$ K as “1”. This new functionality can again be understood from the coupling between the VO₂ and SiC particles. The output particle is not well coupled to the input particle for $T_{\text{in}} < T_c$ so that the emitter particle mainly cools the output particle whereas the heating by the presence of the input particle is small. For $T_{\text{in}} > T_c$ the coupling between the input particle and the output particle is stronger and the heating of the output particle by the input particle is enhanced so that T_{out} makes an upward jump for $T_{\text{in}} > T_c$. We conclude that the transition between the two opposite ports NOT and UNIT can be realized both optically (by using a different nanoparticle) and by acting on the emitter particle temperature T_b , which can thus be seen as a control parameter.

OR gate. We now move to the realization of another basic port, namely the OR logic gate. To this aim we start from the second realization of the UNIT gate, namely the one given in Fig. 2(a) with $T_b = 300$ K, and replace the single VO₂ central particle with two VO₂ particles, obtaining the geometrical configuration described in Fig. 4(b). This is equivalent to having two UNIT gates in parallel. In this configuration, the temperature of the output particle is shown in Fig. 4(c). Since the functionalities of the UNIT gate works for the two input particles separately, the output is clearly that of an OR gate if we define the $T_{\text{out}} > 325$ K as “1” and $T_{\text{out}} < 325$ K as “0”.

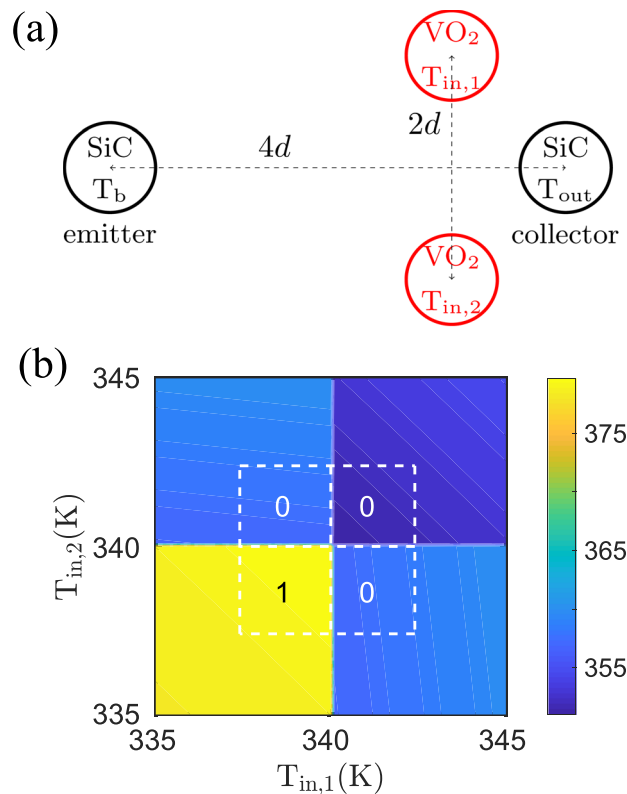


Figure 6. NOR gate. (a) Sketch of the NOR gate configuration. The radii of the nanoparticles is $a = 25$ nm and the interparticle distance between the two input particles is $2d = 200$ nm and between the emitter and collector particle the distance is $4d = 400$ nm whereas the base of the NOT gate is shifted towards the collector of the OR gate such that the distance between them is 100 nm. In this way, we tune the relative coupling strengths such that the effect is relative large. The output temperature of the combined gates, shown in Fig. 5(b), has indeed the signature of a NOR, with a threshold temperature for the output temperature around 375 K. But we have to emphasize that this functionality is due to the fact that the heat flux coming from $T_{b,2}$ is partially absorbed from the input terminals and the bath $T_{b,1}$. When $T_{in,1} > T_c$ or $T_{in,2} > T_c$, this effect increases, cooling down the output particle. In particular, the base particle of the NOT gate is not undergoing any phase transition but stays in its metallic phase. When making the distance between the emitter of the NOT gate and the base larger, then we can bring the base particle to a temperature regime where it makes a phase transition. But in this case, we find that the NOR gate functionality will be lost. This is due to the fact that making the phase transition does not only change the coupling within the NOT gate but also changes the coupling to the particles of the OR gate and therefore results in a completely different configuration. We further want to emphasize that the result in Fig. 5(b) can also be interpreted as a NAND gate when redefining the range of output temperatures for “0” and “1” slightly. Therefore there is some ambiguity. We have tried several other ways of combining individual gates, but it seems that a naive parallel or linear connection does not necessarily result in the expected output. Hence, the main message here is that a circuitry with the basic elements of thermotronics is not obvious. The non-additive nature of radiative heat transfer makes it necessary to design a specific combination of heat-exchanging bodies for each logic output we need to realize.

NOR gate: combination of two ports vs independent realization. After identifying possible configurations of nanoparticles which define fundamental logic gates, it is natural to address the problem of the combination of individual logic gates. With this respect, the issue of non-additivity of radiative heat flux is expected to play a role. We quantitatively address this problem in this section. To this aim, we start from the simple combination of an OR gate and a NOT gate as sketched in Fig. 5(a). The emitter and collector of the NOT gate have this time a relatively large distance of 400 nm whereas the base of the NOT gate is shifted towards the collector of the OR gate such that the distance between them is 100 nm. In this way, we tune the relative coupling strengths such that the effect is relative large. The output temperature of the combined gates, shown in Fig. 5(b), has indeed the signature of a NOR, with a threshold temperature for the output temperature around 375 K. But we have to emphasize that this functionality is due to the fact that the heat flux coming from $T_{b,2}$ is partially absorbed from the input terminals and the bath $T_{b,1}$. When $T_{in,1} > T_c$ or $T_{in,2} > T_c$, this effect increases, cooling down the output particle. In particular, the base particle of the NOT gate is not undergoing any phase transition but stays in its metallic phase. When making the distance between the emitter of the NOT gate and the base larger, then we can bring the base particle to a temperature regime where it makes a phase transition. But in this case, we find that the NOR gate functionality will be lost. This is due to the fact that making the phase transition does not only change the coupling within the NOT gate but also changes the coupling to the particles of the OR gate and therefore results in a completely different configuration. We further want to emphasize that the result in Fig. 5(b) can also be interpreted as a NAND gate when redefining the range of output temperatures for “0” and “1” slightly. Therefore there is some ambiguity. We have tried several other ways of combining individual gates, but it seems that a naive parallel or linear connection does not necessarily result in the expected output. Hence, the main message here is that a circuitry with the basic elements of thermotronics is not obvious. The non-additive nature of radiative heat transfer makes it necessary to design a specific combination of heat-exchanging bodies for each logic output we need to realize.

In the specific case of a NOR gate, we can realize it by using the same idea allowing us to design an OR gate starting from a UNIT one. We can simply use two NOT gates in parallel, by replacing its input particle by two input particles as shown in Fig. 6(a). In this configuration the temperature of the output particle is shown in Fig. 6(b) as a function of the two input temperatures. In analogy with what we have seen before for the UNIT/OR gates, the functionalities of the NOT gate works for the two input particles separately, the output is clearly that of a NOR gate if we define the $T_{out} > 370$ K as “1” and $T_{out} < 370$ K as “0”. It should be noted that by a slightly different definition of the output temperature deciding between “0” and “1” the gate in Fig. 6(b) could as well be interpreted as a NAND gate.

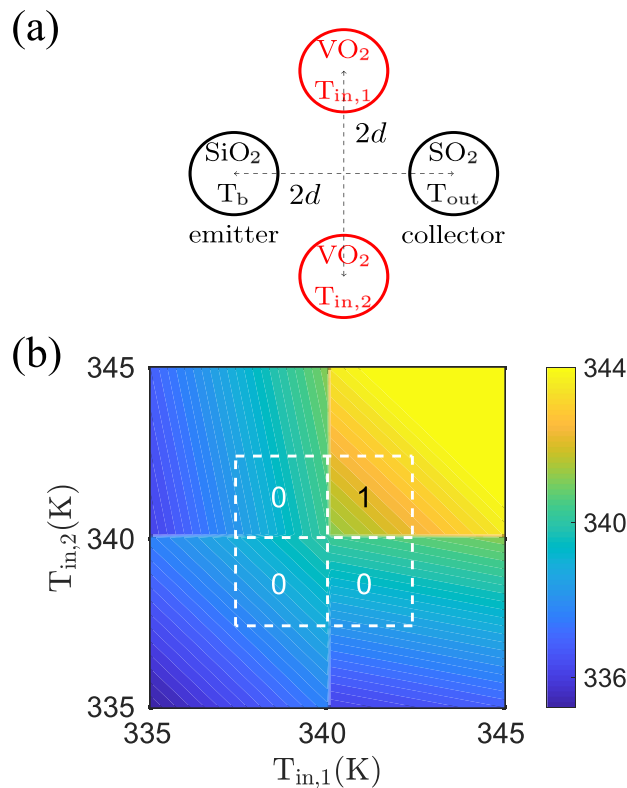


Figure 7. AND gate. (a) Sketch of the AND gate configuration. The radii of the nanoparticles is $a = 25$ nm and the interparticle distance between the two input particles and between the emitter and collector particle is $2d = 200$ nm and $T_b = 400$ K. (b) Output temperature as function of the two input temperatures $T_{in,1,2}$.

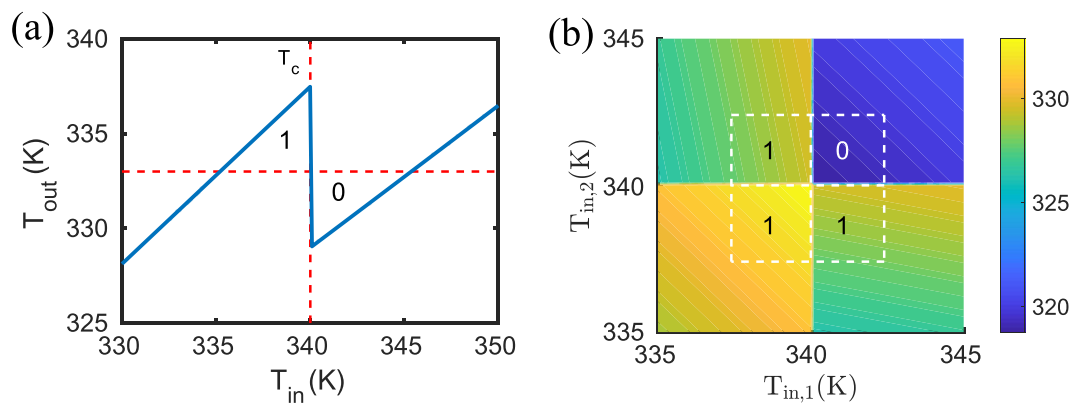


Figure 8. NOT and NAND gate. (a) The output temperature of the configuration in Fig. 3(a) with $T_b = 300$ K. The functionality is that of a NOT gate for logical operations. (b) The output temperature of the configuration in Fig. 7(a) with $T_b = 300$ K. The functionality is that of a NAND gate.

We conclude by giving one clear example of failure of the simple combination of logic gates due to non additivity of radiative heat transfer. As a matter of fact, if we realize a combination of gates as in Fig. 5(a), but with $T_{b,1} = 400$ K and $T_{b,2} = 400$ K, i.e. we combine a NOR and a NOT gate, we obtain again the temperature scheme of a NOR gate (not shown), and not the OR we would expect. This confirms once more the need for an appropriate design of the desired logical operation and the limitations induced by non additivity.

AND and NAND gate. As can be expected from the previous discussion of the NOR gate, we can expect to realize an AND gate by putting two UNIT gates in parallel, which amounts to replace the SiC particles in the NOR gate by SiO_2 particles. Indeed, as shown in Fig. 7 this results in an AND gate. In the same manner as before we can invert the functionality of the UNIT gate and therefore also of the AND gate by using $T_b = 300$ K instead of $T_b = 400$ K. The resulting NOT gate using SiO_2 particles and the NAND gate are shown in Fig. 8.

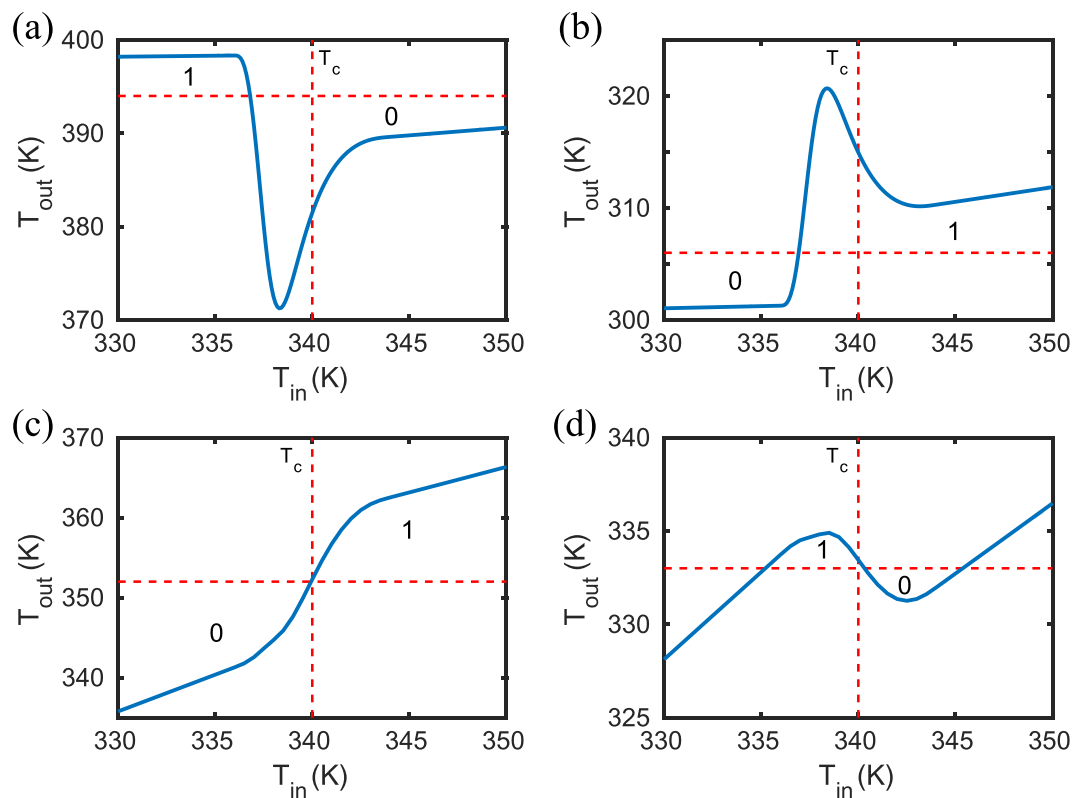


Figure 9. Finite phase transition region. NOT and UNIT gates with a finite transition region for $T \in [336 \text{ K}, 344 \text{ K}]$. The gates with SiC [see (a) and (b)] as output particles are the same as configurations corresponding to Figs. 2(b) and 4(b) and the gates with SiO₂ [see (c) and (d)] as output particles are the same configurations corresponding to Figs. 8(a) and 3(b).

Impact of the width of the VO₂ phase-transition region. In the previous calculations we neglected that the phase transition extends over a range of several degrees and we have further neglected the hysteresis³⁵. The impact of the extended region for the phase transition will of course limit the region where we can clearly define the “0” or “1” to the region outside the phase transition region. Furthermore, due to the hysteresis effect, this transition region will be slightly shifted when cooling the VO₂ particles compared to the case where they are heated. Therefore, depending on the way the logic gates are used, the temperature range in which the gate operates will be slightly different. A detailed analysis of the dynamics of the logic gates, the impact of the extended transition region and the hysteresis effect is out of the scope of the present work and will be done elsewhere.

Here for convenience we illustrate the effect of an extended phase transition region only for the NOT and UNIT gates realized with SiC and SiO₂, respectively. To this end, we model the permittivity of VO₂ in the transition region by the effective medium expression

$$\epsilon_{\text{VO}_2}^{\text{eff}} = (1 - f)\epsilon_{\text{VO}_2}^{\text{d}} + f\epsilon_{\text{VO}_2}^{\text{m}}, \quad (6)$$

where $\epsilon_{\text{VO}_2}^{\text{d/m}}$ are the permittivities of VO₂ in the dielectric/metallic phase. The filling factor $f \in [0, 1]$ can be modeled in different ways. Here we use a so called smoother step function

$$f(x) = 6x^5 - 15x^4 + 10x^3 \quad (7)$$

with $x \in [0, 1]$ realising a smooth transition from 0 to 1. To model the transition in the temperature region $T \in [336 \text{ K}, 344 \text{ K}]$ we use $x = (T - 336 \text{ K})/8 \text{ K}$. The results for the NOT and UNIT gates are shown in Fig. 9.

For the SiO₂-based gates in Fig. 9(c,d) we simply obtain a smoothed transition of the jumps at T_c observed in Figs. 3 and 8(a). Interestingly, for the SiC-based gates we have a non-monotonous transition in Fig. 9(a,b). It turns out that there is an optimal coupling at a filling fraction of $f = 0.18$ which corresponds in our model for $f(x)$ to a temperature of 338.5 K. Due to this optimal coupling there is a minimum in the NOT gate in Fig. 9(a) and a maximum in the UNIT gate in Fig. 9(b) because at this filling fraction the input VO₂ particle optimally cools or heats the SiC output particle, resp. Anyway, when defining the transition temperature defining “0” and “1” of the output by the vertical dashed lines in Fig. 9(a,b) we find that the modelling of the finite transition region shifts the temperature at which the gates switch to temperatures smaller than T_c . In our model the switching of the gates happens at approximately 338 K instead of $T_c = 340 \text{ K}$.

Conclusions

We have introduced here basic scalable circuits to make NOT, OR, NOR, AND and NAND gates from heat flux exchanged in near-field regime in simple nanoparticle networks made with phase change materials. Like in electronics, the NOR gate is obtained by a parallel arrangement of NOT gates. We have shown that the NOT, NOR and AND gate functionalities can be inverted by simply tuning the temperature of surrounding bath around the critical temperature of phase change material.

The development of thermal circuits based on the combination of logic gates should open the door to innovative solutions for an active thermal management of heat flux generated at nanoscale in solid materials. In a long-term perspective, this thermotronics should allow the development of smart systems to take decisions and act using heat flux rather than electricity and even to allow machine-to-machine communication with heat. Potential applications are the zero-electricity presence and movement monitoring of an object using thermal sensors and actuators exposed to the infrared radiation coming from the object. This signal could sequentially activate logic gates, launching a series of boolean operations to analyze the thermal signals, without any other external power making this technology autonomous. For information processing this speed is obviously not competitive with the current electronics devices but it is more than enough for active thermal management and thermal sensing. Moreover, the use of 2D materials with extremely weak heat capacity or systems out of thermal equilibrium could in the next few years drastically reduce the operating speed of thermal circuits.

Received: 6 December 2019; Accepted: 13 February 2020;

Published online: 27 February 2020

References

1. Tsai, C. Y., Kuo, W. T., Lin, C. B. & Chen, T. L. Design and fabrication of MEMS logic gates. *J. Micromech. Microeng.* **18**, 045001 (2008).
2. Singh, P., Tripathi, D. K., Jaiswal, S. & Dixit, H. K. All-Optical Logic Gates: Designs, Classification, and Comparison. *Adv. Opt. Technol.* **2014**, 275083 (2014).
3. Endy, D. Foundations for engineering biology. *Nature* **438**(7067), 449–453 (2005).
4. Moe-Behrens, G. H. The biological microprocessor, or how to build a computer with biological parts. *Comput. Struct. Biotechnol. J.* **7**, e201304003 (2013).
5. Wang, L. & Li, B. Thermal Logic Gates: Computation with Phonons. *Phys. Rev. Lett.* **99**, 177208 (2007).
6. Ghanekar, A., Ricci, M., Tian, Y., Gregory, O. & Zheng, Y. Strain-induced modulation of near-field radiative transfer. *Appl. Phys. Lett.* **112**, 241104 (2018).
7. Biehs, S.-A., Rosa, F. S. S. & Ben-Abdallah, P. Modulation of near-field heat transfer between two gratings. *Appl. Phys. Lett.* **98**, 243102 (2011).
8. Elzouka, M. & Ndao, S. High Temperature Near-Field NanoThermoMechanical Rectification. *Sci. Rep.* **7**, 44901 (2017).
9. Huang, Y., Boriskina, S. V. & Chen, G. Electrically tunable near-field radiative heat transfer via ferroelectric materials. *Appl. Phys. Lett.* **105**, 244102 (2014).
10. Messina, R., Ben-Abdallah, P., Guizal, B. & Antezza, M. Graphene-based amplification and tuning of near-field radiative heat transfer between dissimilar polar materials. *Phys. Rev. B* **96**, 045402 (2017).
11. Ilic, O. *et al.* Active Radiative Thermal Switching with Graphene Plasmon Resonators. *ACS Nano* **12**, 2474 (2018).
12. Shi, K., Bao, F. & He, S. Enhanced Near-Field Thermal Radiation Based on Multilayer Graphene-hBN Heterostructures. *ACS Photonics* **4**, 971 (2017).
13. Yi, X.-J. *et al.* Near-field radiative heat transfer between black phosphorus and graphene sheet. *Mat. Res. Express* **6**, 025906 (2019).
14. Moncada-Villa, E., Fernandez-Hurtado, V., García-Vidal, F. J., García-Martin, A. & Cuevas, J. C. Magnetic field control of near-field radiative heat transfer and the realization of highly tunable hyperbolic thermal emitters. *Phys. Rev. B* **92**, 125418 (2015).
15. Zhu, L. & Fan, S. Persistent Directional Current at Equilibrium in Nonreciprocal Many-Body Near Field Electromagnetic Heat Transfer. *Phys. Rev. Lett.* **117**, 134303 (2016).
16. Latella, I. & Ben-Abdallah, P. Giant Thermal Magnetoresistance in Plasmonic Structures. *Phys. Rev. Lett.* **118**, 173902 (2017).
17. Abraham, E. R. M., Ben-Abdallah, P., Cuevas, J. C. & García-Martin, A. Anisotropic Thermal Magnetoresistance for an Active Control of Radiative Heat Transfer. *ACS Photonics* **5**, 705 (2017).
18. Ben-Abdallah, P. Photon Thermal Hall Effect. *Phys. Rev. Lett.* **116**, 084301 (2016).
19. Ott, A., Messina, R., Ben-Abdallah, P. & Biehs, S.-A. Magnetothermoplasmonics: from theory to applications. *J. Photon. Energy* **9**, 032711 (2019).
20. Wu, H., Huang, Y., Cui, L. & Zhu, K. Active Magneto-Optical Control of Near-Field Radiative Heat Transfer between Graphene Sheets. *Phys. Rev. Appl.* **11**, 054020 (2019).
21. Zheng, Z. & Xuan, Y. Near-field radiative heat transfer between general materials and metamaterials. *Chinese Science Bulletin* **56**, 2312 (2011).
22. Iizuka, H. & Fan, S. Rectification of evanescent heat transfer between dielectric-coated and uncoated silicon carbide plates. *J. Appl. Phys.* **112**, 024304 (2012).
23. Ben-Abdallah, P. & Biehs, S.-A. Phase-change radiative thermal diode. *Appl. Phys. Lett.* **103**, 191907 (2013).
24. Yang, Y., Basu, S. & Wang, L. Radiation-based near-field thermal rectification with phase transition materials. *Appl. Phys. Lett.* **103**, 163101 (2013).
25. Ito, K., Nishikawa, K., Iizuka, H. & Toshiyoshi, H. Experimental investigation of radiative thermal rectifier using vanadium dioxide. *Appl. Phys. Lett.* **105**, 253503 (2014).
26. Ito, K., Nishikawa, K., Miura, A., Toshiyoshi, H. & Iizuka, H. Dynamic Modulation of Radiative Heat Transfer beyond the Blackbody Limit. *Nano Lett.* **17**, 4347 (2017).
27. Fiorino, A. *et al.* A Thermal Diode Based on Nanoscale Thermal Radiation. *ACS Nano* **12**, 5774 (2018).
28. Otey, C. R., Lau, W. T. & Fan, S. Thermal Rectification through Vacuum. *Phys. Rev. Lett.* **104**, 154301 (2010).
29. Basu, S. & Francoeur, M. Near-field radiative transfer based thermal rectification using doped silicon. *Appl. Phys. Lett.* **98**, 113106 (2011).
30. Wang, L. P. & Zhang, Z. M. Thermal Rectification Enabled by Near-Field Radiative Heat Transfer Between Intrinsic Silicon and a Dissimilar Material. *Nanoscale and Microscale Thermophysical Engineering* **17**, 337 (2013).
31. Nefzaoui, E., Joulain, K., Drevillon, J. & Ezzahri, Y. Radiative thermal rectification using superconducting materials. *Appl. Phys. Lett.* **104**, 103905 (2014).
32. Ordonez-Miranda, J., Joulain, K., De Sousa Meneses, D., Ezzahri, Y. & Drevillon, J. Photonic thermal diode based on superconductors. *J. Appl. Phys.* **122**, 093105 (2017).

33. Ott, A., Messina, R., Ben-Abdallah, P. & Biehs, S.-A. Radiative thermal diode driven by nonreciprocal surface waves. *Appl. Phys. Lett.* **114**, 163105 (2019).
34. Ben-Abdallah, P. & Biehs, S.-A. Near-Field Thermal Transistor. *Phys. Rev. Lett.* **112**, 044301 (2014).
35. Ordóñez-Miranda, J., Ezzahri, Y., Drevillon, J. & Joulain, K. Transistorlike Device for Heating and Cooling Based on the Thermal Hysteresis of VO₂. *Phys. Rev. Appl.* **6**, 054003 (2016).
36. Kubyt'skiy, V., Biehs, S.-A. & Ben-Abdallah, P. Radiative Bistability and Thermal Memory. *Phys. Rev. Lett.* **113**, 074301 (2014).
37. Dyakov, S. A., Dai, J., Yan, M. & Qiu, M. Near-field thermal memory based on radiative phase bistability of VO₂. *J. Phys. D: Appl. Phys.* **48**, 305104 (2015).
38. Khandekar, C. & Rodriguez, A. W. Thermal bistability through coupled photonic resonances. *Appl. Phys. Lett.* **111**, 083104 (2017).
39. Latella, I., Marconot, O., Sylvestre, J., Fréchet, L. G. & Ben-Abdallah, P. Dynamical Response of a Radiative Thermal Transistor Based on Suspended Insulator-Metal-Transition Membranes. *Phys. Rev. Applied* **11**, 024004 (2019).
40. Ben-Abdallah, P. & Biehs, S.-A. Towards Boolean operations with thermal photons. *Phys. Rev. B* **94**, 241401(R) (2016).
41. Becerril, D. & Noguez, C. Near-field energy transfer between nanoparticles modulated by coupled multipolar modes. *Phys. Rev. B* **99**, 045418 (2019).
42. Messina, R., Tschikin, M., Biehs, S.-A. & Ben-Abdallah, P. Fluctuation-electrodynamics theory and dynamics of heat transfer in systems of multiple dipoles. *Phys. Rev. B* **88**, 104307 (2013).
43. Dong, J., Zhao, J. & Liu, L. Radiative heat transfer in many-body systems: Coupled electric and magnetic dipole approach. *Phys. Rev. B* **95**, 125411 (2017).
44. Ekeröth, R. M. A., García-Martin, A. & Cuevas, J. C. Thermal discrete dipole approximation for the description of thermal emission and radiative heat transfer of magneto-optical systems. *Phys. Rev. B* **95**, 235428 (2017).
45. Novotny, L. & Hecht, B. "Principles of Nano-Optics", (Cambridge University Press, New York, 2012).
46. Säskiläthi, K., Oksanen, J. & Tulkki, J. Quantum Langevin equation approach to electromagnetic energy transfer between dielectric bodies in an inhomogeneous environment. *Phys. Rev. B* **89**, 134301 (2014).
47. Asheichyk, K., Müller, B. & Krüger, M. Heat radiation and transfer for point particles in arbitrary geometries. *Phys. Rev. B* **96**, 155402 (2017).
48. Dong, J., Zhan, J. & Liu, L. Long-distance near-field energy transport via propagating surface waves. *Phys. Rev. B* **97**, 075422 (2018).
49. Messina, R., Biehs, S.-A. & Ben-Abdallah, P. Surface-mode-assisted amplification of radiative heat transfer between nanoparticles. *Phys. Rev. B* **97**, 165437 (2018).
50. Albaladejo, S. *et al.* Radiative corrections to the polarizability tensor of an electrically small anisotropic dielectric particle. *Opt. Express* **18**, 3556 (2010).
51. Ben-Abdallah, P., Biehs, S.-A. & Joulain, K. Many-Body Radiative Heat Transfer Theory. *Phys. Rev. Lett.* **107**, 114301 (2011).
52. Edalatpour, S. & Francoeur, M. The Thermal Discrete Dipole Approximation (T-DDA) for near-field radiative heat transfer simulations in three-dimensional arbitrary geometries. *J. Quant. Spectr. Radiat. Transfer* **133**, 364 (2014).
53. Edalatpour, S., Cuma, M., Trueax, T., Backman, R. & Francoeur, M. Convergence analysis of the thermal discrete dipole approximation. *Phys. Rev. E* **91**, 063307 (2015).
54. Handbook of Optical Constants of Solids, edited by E. Palik (Academic Press, New York, 1998).
55. Qazilbash, M. M. *et al.* Mott Transition in VO₂ Revealed by Infrared Spectroscopy and Nano-Imaging. *Science* **318**, 1750 (2007).

Acknowledgements

S.-A.B. acknowledges support from Heisenberg Programme of the Deutsche Forschungsgemeinschaft (DFG, German Research Foundation) under the project No. 404073166.

Author contributions

C.K. performed the numerical simulations. All the authors discussed the results and contributed to the preparation of the manuscript.

Competing interests

The authors declare no competing interests.

Additional information

Correspondence and requests for materials should be addressed to S.-A.B.

Reprints and permissions information is available at www.nature.com/reprints.

Publisher's note Springer Nature remains neutral with regard to jurisdictional claims in published maps and institutional affiliations.



Open Access This article is licensed under a Creative Commons Attribution 4.0 International License, which permits use, sharing, adaptation, distribution and reproduction in any medium or format, as long as you give appropriate credit to the original author(s) and the source, provide a link to the Creative Commons license, and indicate if changes were made. The images or other third party material in this article are included in the article's Creative Commons license, unless indicated otherwise in a credit line to the material. If material is not included in the article's Creative Commons license and your intended use is not permitted by statutory regulation or exceeds the permitted use, you will need to obtain permission directly from the copyright holder. To view a copy of this license, visit <http://creativecommons.org/licenses/by/4.0/>.

© The Author(s) 2020